

Comparing structural, morphological, and optical properties of PS/TiO₂ nanocomposite films prepared by the dip coating and electrospinning methods

S. A. A. AL Saati^{1,2*}, Najmeddine Abdelmoula², Mohammed Hadi Shinen³

¹College of Basic Education, University of Babylon, Babylon, Iraq

²University of Sfax, Faculty of Sciences of Sfax, Laboratory of Multifunctional Materials and Applications, Tunisia

³College of Science, University of Babylon, Babylon 51002, Iraq

*Corresponding author e-mail: basic.safer.abd@uobabylon.edu.iq

Abstract. This study included the preparation of pure polystyrene (PS) and PS/TiO₂ nanocomposites with varying concentrations (2, 4, and 6 wt.%) of titanium dioxide nanoparticles (TiO NPs). The TiO NPs were generated using both the immersion and the electrospinning methods. X-ray diffraction (XRD) analysis showed that polystyrene is amorphous and no clear peaks corresponding to TiO NPs were found. The Fourier transform infrared spectroscopy (FTIR) analysis revealed no discernible interaction between TiO NPs and PS. Atomic force microscopy (AFM) analysis demonstrated that incorporating TiO NPs into PS has non-uniform surface distribution. As evidenced by the scanning electron microscopy (SEM) images of the samples obtained by the dip coating technique, agglomerated and layered spherical particles were observed. However, the samples synthesized by the electrospinning method showed that the TiO NPs were well-dispersed, and no agglomerations related to the TiO NPs were detected. The study using UV-visible spectrophotometry showed a positive correlation between the concentration of TiO NPs and the absorbance in both samples prepared by the dip coating and electrospinning methods. The increment in the volume fraction of the TiO NPs resulted in a decrement in the band gap energy of the samples prepared by the dip coating and electrospinning methods, implying that the electron transition from the valence band to the conduction one can be simplified by increasing the concentration of TiO₂ nanoparticles.

Keywords: PS/TiO₂ nanocomposite, dip coating, electrospinning, optical properties, polystyrene, TiO₂.

<https://doi.org/10.15407/spqeo28.02.147>

PACS 61.05.cp, 61.72.Dd, 68.37.Hk, 78.66.Qn

Manuscript received 24.12.24; revised version received 16.03.25; accepted for publication 11.06.25; published online 26.06.25.

1. Introduction

Over the past two decades, polymer nanocomposites have attracted substantial attention because they not only have several fascinating properties, namely low weight [1], cost-efficiency and ease-of-synthesis [2, 3], but they also possess multi-faceted, multi-functional capabilities suitable for a wide range of applications, especially in the area of printed electronics [4, 5]. Polymer nanocomposites contain polymer or copolymer with nanoparticles embedded in the polymer matrix [6, 7]. Combining the distinguished properties of polymers and nanoparticles in unique well-designed composites leads to creating materials of great interest from fundamental and technological points of view [8, 9]. Polystyrene (PS) is widely used due to its useful characteristics like low cost, lightweight, and ease of manufacture [10, 11].

Titanium dioxide (TiO₂) is considered one of the most excellent photocatalytic materials due to its low cost, less toxicity, and high photocatalytic activities [12, 13]. TiO₂-like films have been prepared by different methods, namely DC and RF reactive magnetron sputtering, electron beam evaporation, ion beam assisted deposition, sol-gel method chemical vapor deposition, electrodeposition, pulsed laser deposition, and spray pyrolysis [14–18]. Because of their intriguing optical, electrical, and chemical characteristics, TiO₂-based photocatalytic thin films and nanostructures are now widely used for several applications, including antibacterial material, water splitting, and remediation of the environment [19]. Different mechanical, chemical, and physical surface functions, namely increased surface area and improved photocatalytic activity, can be achieved by engineering thin films at the nanoscale [20].

The field of PS nanocomposites has gained significant attention due to the substantial improvement in the mechanical and thermal properties of the polymer resulting from the incorporation of small quantities of nanoparticles [21]. Nevertheless, information is scarce regarding the photodegradation characteristics of PS nanocomposites, as stated in reference [22].

The authors El-Aasser *et al.* [23] synthesized hybrids of polymer and TiO₂ through the utilization of OLOA 370 as a stabilizer composed of polyisobutene succinamide, polybutene-succinimide pentamine, as a surface modifier for nano-titania. This was followed by the dispersion of TiO₂ into the monomer. The preparation of composite structures consisting of a polymer core and an inorganic shell involves the typical approach of the initial preparation of polymer spheres through polymerization. Subsequently, these spheres are transferred to a solvent environment where organic TiO₂ precursors are introduced to facilitate the formation of thin TiO₂ particles. Incorporating pre-synthesized TiO₂ dispersion into miniemulsion before polymerization is a tactic during the fabrication of PS/TiO₂. Liu *et al.* applied a coating of TiO₂ nanoparticles onto polystyrene cores, which were pre-prepared, using acrylic acid as a comonomer. This method was found to enhance the interaction between the TiO₂ and polymer cores.

Toyama and his colleagues [24] synthesized PS/TiO₂ core-shell particles and examined their photocatalytic activity concerning the decomposition of methylene blue (MB). The coating of the PS particles with TiO₂ was done using the sol-gel method. The decomposition of MB by the PS/TiO₂ core-shell particles after 24 min was 87%, which was higher than that of the prepared TiO₂ (60%) and the commercial P25 (58%). The excellent performance of PS/TiO₂ core-shell particles concerning the decomposition of MB was attributed to the crystallinity and shell thickness of TiO₂ on the surface of PS particles [24]. In another study [25], PS/TiO₂ composites were fabricated to examine their photocatalytic performance concerning the removal of ciprofloxacin (CIP) used as an antibiotics from wastewater. Various parameters, including the amount of polymer, pH and the initial CIP concentration were investigated on the performance of the synthesized composites concerning the degradation of the CIP. The maximum removal of CIP was 95%. The inclusion of PS into TiO₂ has resulted in the removal of the barriers faced by TiO₂ nanoparticles when they were used alone [25].

Jaleh *et al.* [26] fabricated PS-TiO₂ nanocomposites by spin coating method from a solution of PS in which the TiO₂ nanoparticles were dispersed with mechanical mixing. The incorporation of TiO₂ nanoparticles into the PS has led to a decrement in its optical band gap. It means that TiO₂ nanoparticles can improve the photocatalytic performance of PS [26]. In this paper, PS/TiO₂ nanocomposites were prepared by the two processes: dip coating and electro-spin coating methods and their structural, morphological, and optical properties were investigated.

2. Materials and methods

Pure polystyrene (PS, Reagent World in the USA) with a molecular weight of 281,000 g/mol (GPC), as well as titanium dioxide nanoparticles with particle size < 26 nm (TiO₂ NPs, HIMEDIA, India), chloroform (CHCl₃, HIMEDIA, 99.0%) and de-ionized water were used in this study.

2.1. Preparation of PS/TiO₂ nanocomposite

The TiO₂ NPs of different weight percentages (2%, 4%, and 6%) were effectively dissolved using 6 mL of absolute chloroform. The resultant solution was subjected to ultrasonic mixing for 20 min to form a homogeneous mixture. The ultrasonic bath used in the synthesis procedure was the Grant XUBA5 model, equipped with a heating capability of 150 W. Thereafter, the mixture was subjected to magnetic stirring for 2 hours to inhibit the formation of agglomerates. The composites, consisting of 2%, 4% or 6% TiO₂/PS nanoparticles, were fabricated using two distinct techniques: electrospinning and dip coating.

2.2. Electrospinning process

The electrospinning process was carried out under ambient conditions, with a voltage of 28 kV, a distance of 50 mm, a turntable speed of 1500 rpm, and an injection rate varying from 0.07 to 0.1 mm/h. A fine wire mesh with a small hole size was used to separate large polymer agglomerates before measuring the dispersion viscosity. The experimental setup for electrospinning consists of a glass chamber containing a solution, equipped with a nozzle and a metal needle, along with aluminium foil and the Simco Chagemaster BP 50 voltage source. The experimental setup was positioned in a fume chamber. The tin plate and the nozzle were affixed to separate stands with the capability to adjust the working distance (distance between the needle tip and the collecting plate). The glass slides were affixed to the turntable. The voltage source was connected to the nozzle and the collector, whereby the nozzle was positively charged and the collector plate was negatively charged. Varying the voltage and working distance allows us to change the shape and strength of the generated horizontal electrostatic field. The nozzle exploited needles of varying sizes and lengths. The feeding rate of the dispersion was determined by the combined influence of gravity and the characteristics of the needle. The voltage and distance parameters were independently manipulated for each sample to generate a discernible layer on the substrate.

2.3. Dip coating process

This methodology encompasses a series of sequential procedures, which were carried out at room temperature. The dip coating process lasted approximately 15 min. Initially, the substrate, namely a glass slide, is submerged in a solution that contains the coating material. This immersion process is carried out at a constant velocity of

10 mm/s. The substrate is subsequently immersed in the solution for a specific duration (1 min), thereafter it is vertically withdrawn at a constant velocity of 10 mm/s. The abovementioned procedure was repeated five times to obtain a single sample. Subsequently, the slides are subjected to vertical drying at room temperature.

2.4. Characterization of PS/TiO₂

The morphology of the PS/TiO₂ nanocomposites was analyzed using scanning electron microscope (SEM) images obtained by the JSM 6390 electron scanner at an accelerating voltage of 10 kV. The images were subsequently analyzed using the Image J software. The crystal structure of the nanocomposites was examined using the X-ray diffraction (XRD) method applied with the Swift ED attachment on the JEOL JSM 6390 instrument. Other techniques, namely atomic force microscopy (AFM) and Fourier infrared spectroscopy (FTIR), were also used to characterize nanocomposites. The optical properties of the PS/TiO₂ nanocomposites were studied using a spectrophotometer (UV-18000A-Shimadzu) operating within a wavelength range of 200 to 800 nm. The calculation of the absorption coefficient (α) was performed according to the method outlined in reference [27]:

$$\alpha = 2.303(A/d), \quad (1)$$

where A is the absorbance and d is the thickness.

The energy gap is given by [28]:

$$(\alpha h\nu)^{1/m} = C(h\nu - E_g), \quad (2)$$

where C is constant, $h\nu$ is the photon energy, E_g is the energy gap, $m = 2$ and 3 for allowed and forbidden indirect transitions.

3. Results and discussion

3.1. SEM microscopy

Fig. 1 shows the SEM images of PS and PS/TiO₂ nanocomposites prepared using the dip coating method at varying magnifications. The surface of the pure PS sample depicted in Fig. 1a shows good homogeneity and smoothness, indicating the efficiency of the procedure used for the preparation of the sample. Conversely, Figs. 1b–1d exhibit agglomerated and layered spherical particles. Nevertheless, the granular size is smaller than 10 μm , which correlates well with the results of [29].

Fig. 2 presents the SEM images of pure PS and PS/TiO₂ nanocomposite samples synthesized using electrospinning. The images were obtained at various magnifications. The PS and PS/TiO₂ fibers exhibit smooth surfaces without irregularities, and TiO₂ agglomerations were not detected on the fiber surfaces. This observation indicates the uniform distribution of TiO₂ nanoparticles along the spun nanofibers caused by the action of ultrasound. Consequently, we can conclude that the PS as a viscous medium successfully maintained the nanoparticles in a suspended form during the

electrospinning process. This peculiarity suggests that the electrospinning technique effectively produced fibers without separating TiO₂ particles from the PS medium. This SEM study yielded favorable outcomes, demonstrating that the average fiber diameter is within 541...498 nm, with a minimum of 460 nm. These findings suggest that the incorporation of nanoparticles has a substantial impact on the final size of fibers, which correlate well with the results in [30].

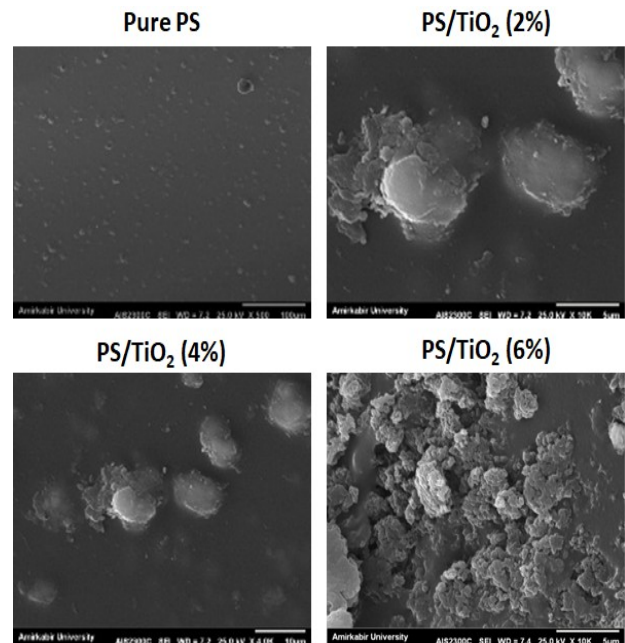


Fig. 1. SEM images of pure PS, PS/TiO₂ (2 wt.%), PS/TiO₂ (4 wt.%), and PS/TiO₂ (6 wt.%) provided by dip coating method.

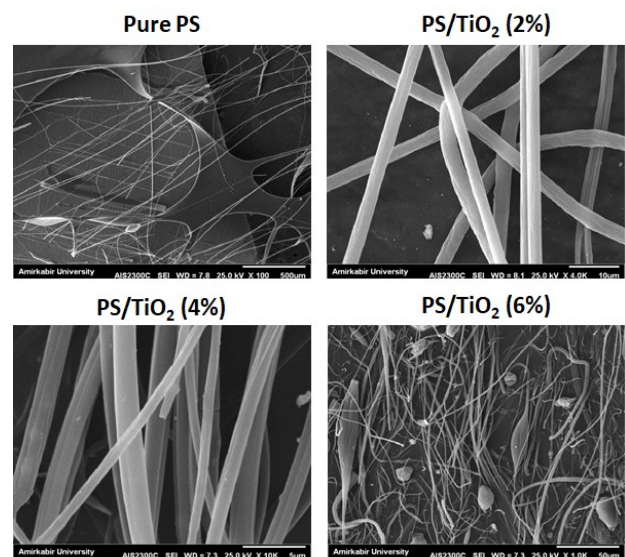


Fig. 2. SEM images of PS/TiO₂ composites using different ratios of titanium dioxide prepared by electrospinning method.

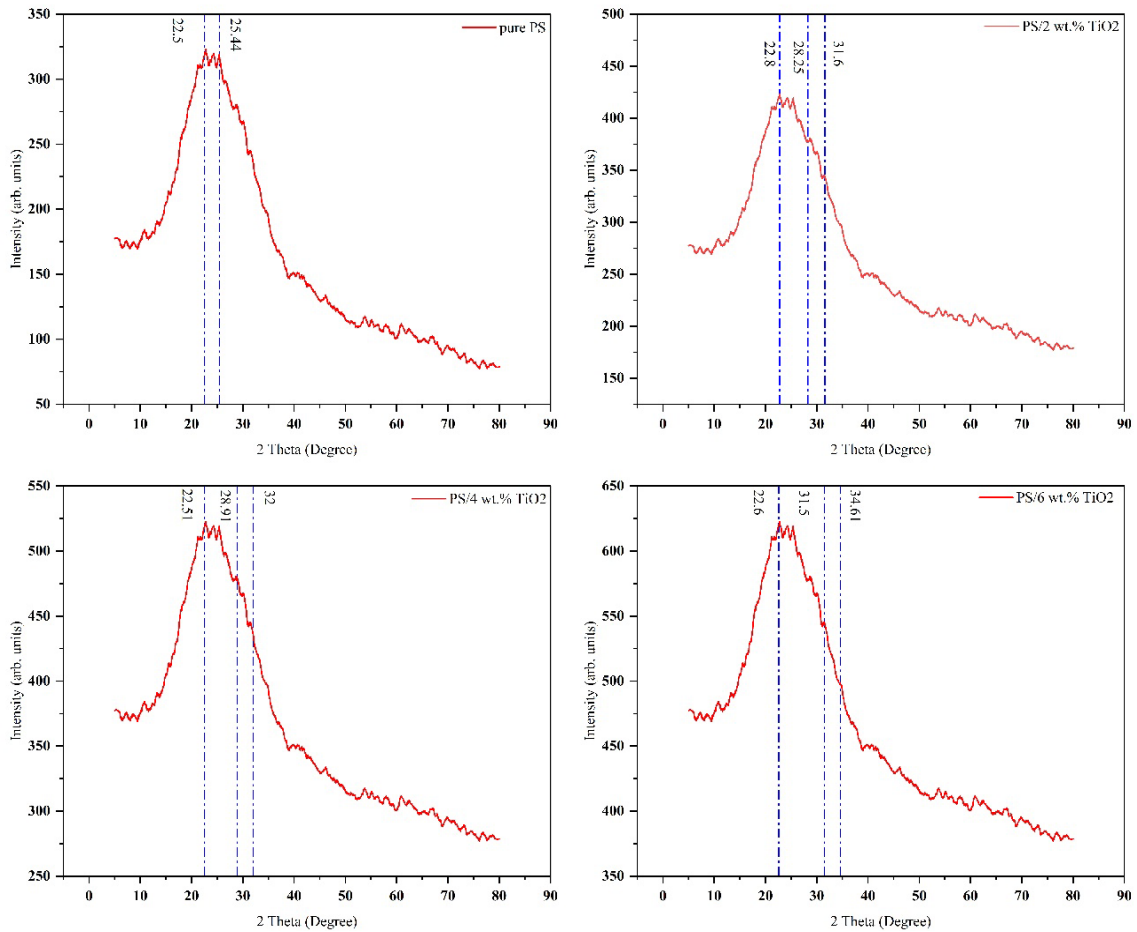


Fig. 3. XRD patterns of PS/TiO₂ composites prepared by electrospinning. For interpretation of the colors in the figures, the reader is referred to the web version of this article.

3.2. XRD analysis

The X-ray diffraction patterns of PS polymer and its nanocomposites are shown in Figs. 3 and 4.

One can see that the pure PS sample exhibits a wide peak within the angle range of 15° to 35° indicating the amorphous structure of polystyrene. At the same time, the diffraction patterns of PS/TiO₂ do not exhibit any

discernible peaks corresponding to TiO₂ NPs, which can be explained by low concentration of TiO₂ in the nanocomposite or the effective dispersion of the nanofibers [24, 26]. The lack of diffraction peaks attributed to TiO₂ nanoparticles can be also explained by the effective integration of TiO₂ into the material, resulting in a reduction in the *d*-spacing that is not discernible as an independent entity by the XRD analysis [31–33].

Table 1. The AFM obtained surface parameters of PS/TiO₂ nanocomposites with different concentrations of TiO₂ NPs obtained using the dip coating and electrospinning.

Sample	Roughness average (nm)	Root mean square (nm)	Ten point height (nm)	Average diameter (nm)
Pure PS D	0.132	0.16	0.462	7.02
PS/2 wt.% D	0.198	0.235	1.3	12.5
PS/4 wt.% D	1.93	2.28	3.84	15
PS/6 wt.% D	5.27	6.46	20.4	17.5
Pure PS E	0.606	0.739	3.4	9
PS/2 wt.% E	0.517	0.611	1.37	16
PS/4 wt.% E	1.14	1.54	4.65	18
PS/6 wt.% E	2.03	2.43	6.51	20

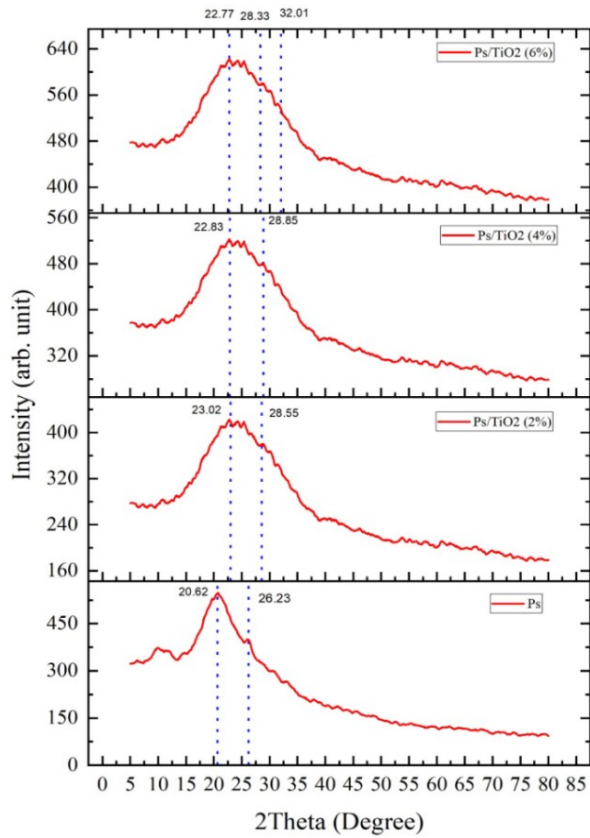


Fig. 4. XRD patterns of PS/TiO₂ composites with various concentrations of TiO₂ prepared by dip coating.

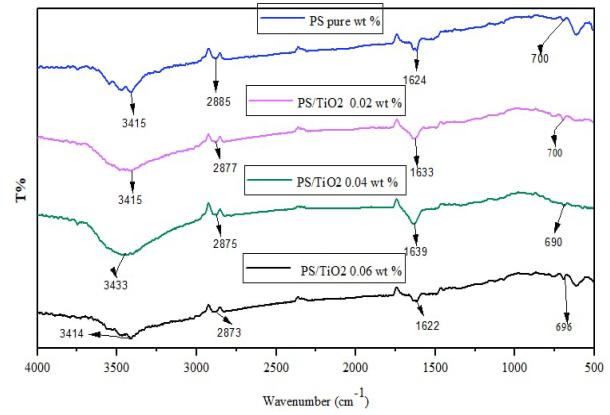


Fig. 5. FTIR spectra of the pure PS and PS/TiO₂ nano-composites with different concentrations of TiO₂.

3.3. FT-IR analysis

The FTIR spectra of both PS and PS/TiO₂ nano-composites are depicted in Fig. 5. The band at 3415 cm⁻¹ in the PS spectrum is caused by the aromatic C–H axial deformation [44]. The vibrational modes at 2885 cm⁻¹ are attributed to the symmetric stretching of CH₂ groups. The band at 1624 cm⁻¹ is commonly associated with the stretching vibration of the phenyl ring. The aromatic C–H out-of-plane deformation manifests itself as the band at 700 cm⁻¹ [35]. The FTIR studies demonstrate that embedding TiO₂ results in the redistribution of certain chemical bonds, rather than the appearance of new spectral peaks. This peculiarity can be explained by

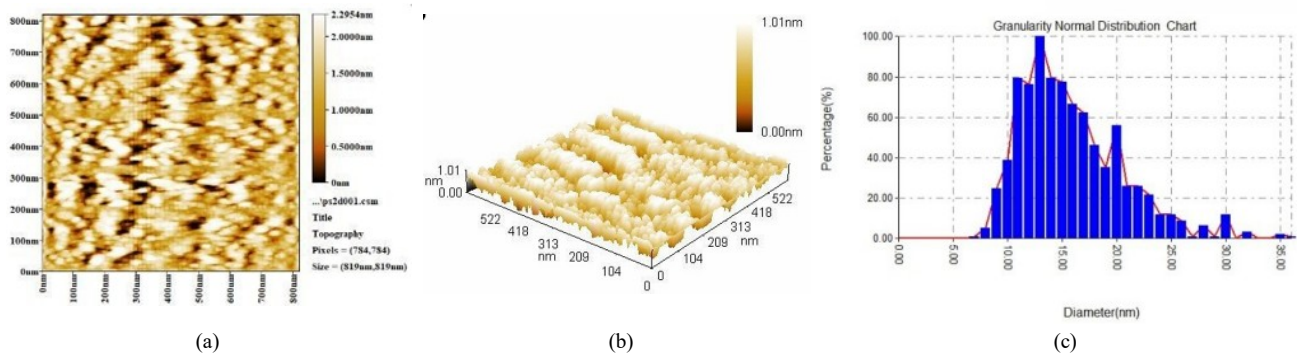


Fig. 6. AFM images of PS/TiO₂ (2 wt.%) prepared using dip coating for 2D (a), 3D (b) and histogram grain (c).

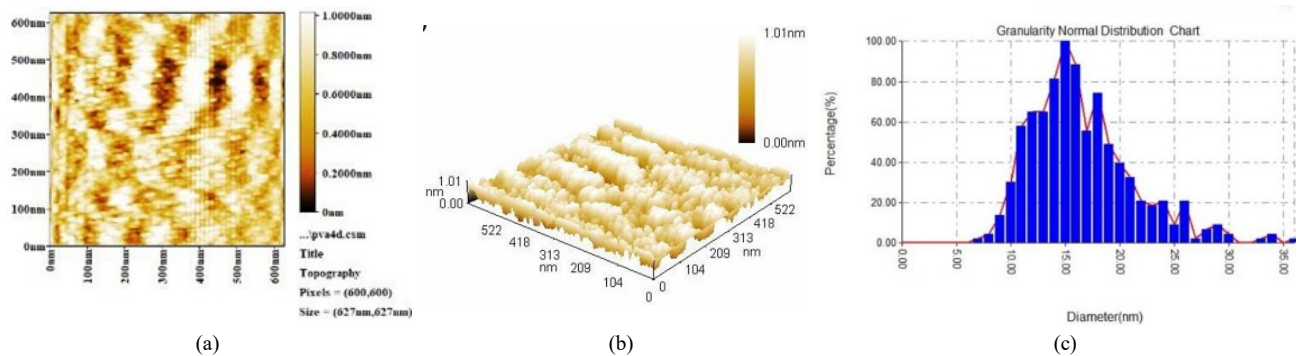


Fig. 7. AFM images of the surface of PS/TiO₂ (6 wt.%) prepared using dip coating for 2D (a), 3D (b), and histogram grain (c).

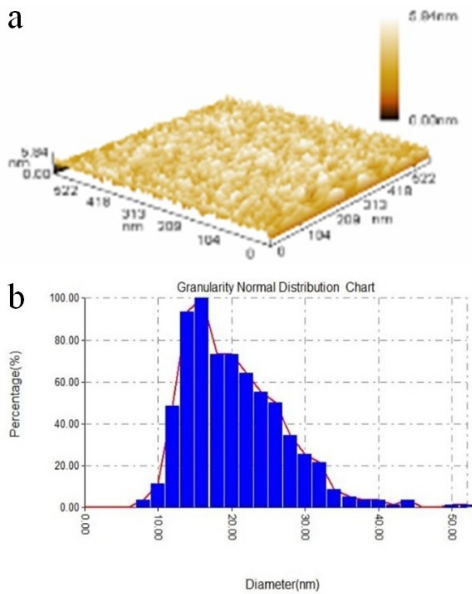


Fig. 8. AFM images of the surface of PS/TiO₂ (2 wt.%) prepared by electrospinning for 3D (a) and the corresponding histogram of grain size (b).

a lack of chemical bonds between TiO₂ nanoparticles and the polystyrene polymer matrix.

3.4. AFM test

Figs. 6–8 depict the AFM images of the surface of PS/TiO₂ nanocomposites (2 and 6 wt.%). Each figure consists of 2D, 3D images, and a histogram representing the grain size distribution.

The AFM images of PS/TiO₂ nanocomposites exhibit a notable degree of surface homogeneity indicating uniform distribution of crystalline granules. The corresponding values of the roughness, root mean square (RMS), ten-point height, and average diameter of the surface grains are collected in Table 1. The white regions in the images manifest the joint crystalline granules, indicating aggregation of the neighboring granules. Consequently, the granules inside the white areas have a larger size compared to those in other locations.

The roughness and RMS values exhibit an increase from 0.16 nm for polystyrene films to 6.46 nm for PS/TiO₂ (6 wt.%) prepared using the dip coating and up to 2.43 nm for PS/TiO₂ (6 wt.%) synthesized using the electrospinning, wherein the adequate surface diffusion facilitated the deposition process. The increase in the RMS resulted in a higher enhancement of crystalline development along the vertical axis compared to the horizontal axis. Table 1 presents the data on the ten-point height and average diameter of crystalline grains.

One can see that the average diameter increases with increasing the concentration of TiO₂ NPs. Particularly, the average diameter varies from 7.02 to 17.5 nm for PS/TiO₂ (6 wt.%) synthesized using the dip coating method, resulting in particle sizes varying from 9 to 20 nm. It is worth noting that TiO₂ was also synthesized using the electrospinning method. Such behavior was documented in previous studies [36, 37].

3.5. UV-Visible analysis

Figs. 9 and 10 depict the absorption spectra of the studied nanocomposites. One can see a correlation between the concentration of TiO₂ NPs and absorbance. In this context, Figs. 11 and 12 illustrate the observed decrease in transmittance with increasing the concentration of TiO₂ NPs.

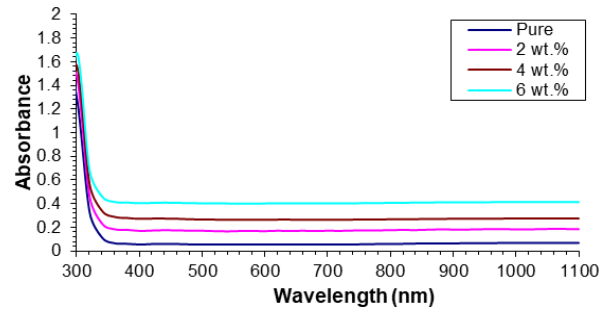


Fig. 9. UV-vis absorption spectra of PS/TiO₂ nanocomposite prepared using dip coating.

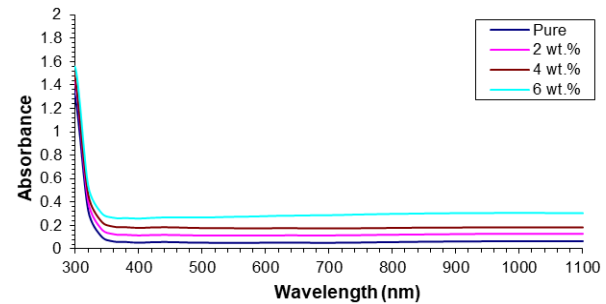


Fig. 10. UV-vis absorption spectra of PS/TiO₂ nanocomposite prepared using electrospinning.

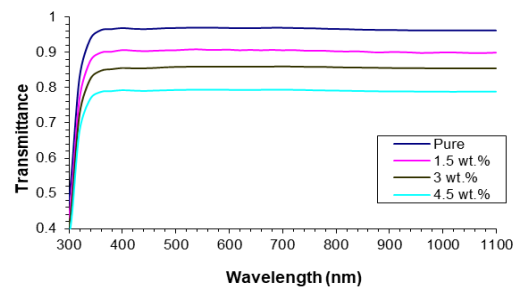


Fig. 11. The transmittance spectra of PS/TiO₂ nanocomposite prepared using dip coating.

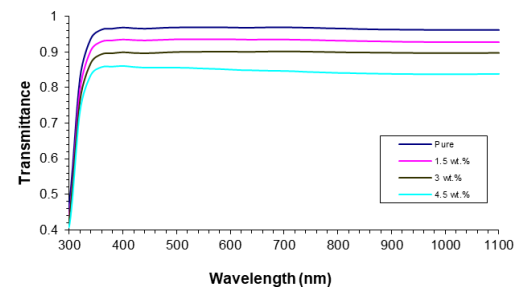


Fig. 12. The transmittance spectra of PS/TiO₂ nanocomposite prepared using electrospinning.

The absorption coefficient (α) was determined using Eq. (1). Figs. 13 and 14 show the absorption coefficient of the PS/TiO₂ nanocomposites under study. One can see that the value of α exhibits an upward trend with increasing the concentration of TiO₂ NPs.

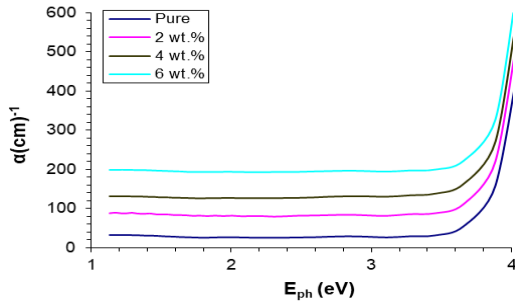


Fig. 13. The absorption coefficient of PS/TiO₂ nanocomposites prepared using dip coating.

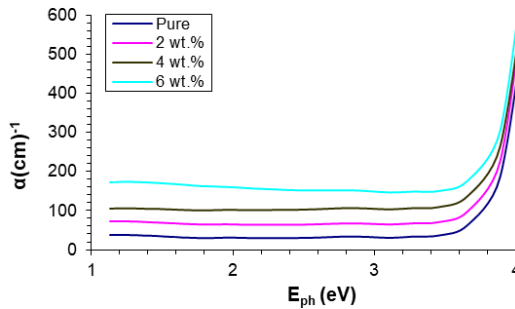


Fig. 14. The absorption coefficient of PS/TiO₂ nanocomposites prepared using electrospinning.

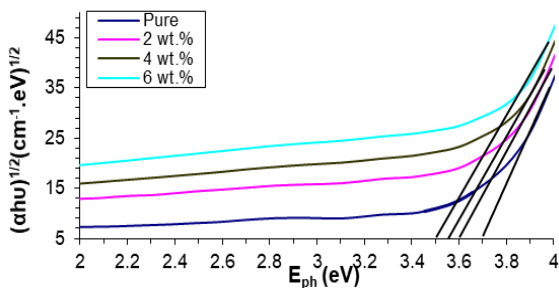


Fig. 15. The Tauc plot for pure PS and PS with different concentrations of TiO₂ NPs prepared by dip coating. The extrapolation of the linear part is performed for the allowed transitions.

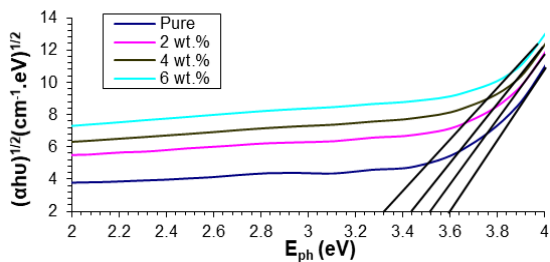


Fig. 16. The Tauc plot for pure PS and PS with different concentrations of TiO₂ NPs prepared by dip coating. The extrapolation of the linear part is performed for the forbidden transitions.

This phenomenon can be attributable to the concurrent increase in absorbance. The absorption coefficient provides insights into the nature of the transition. If the value of α is larger than 104, it indicates the direct transition type. Conversely, if the value of α is smaller than 104, it shows the indirect transition type [39]. In our case, the value of α is below 104 for PS/TiO₂ nanocomposites with concentrations less than 6 wt.% indicating the indirect electron transition.

The calculation of the optical indirect energy band gap was performed using equation (2). Figs. 15 and 16 depict the Tauc plot for the allowed and forbidden transitions in PS/TiO₂ nanocomposites fabricated using the dip coating. The extrapolation of the linear part shows the calculated optical band gap.

The calculation of the optical indirect energy band gap was performed using equation (2). Figs. 15 and 16 depict the Tauc plot for the allowed and forbidden transitions in PS/TiO₂ nanocomposites fabricated using the dip coating. The extrapolation of the linear part shows the calculated optical band gap.

Similarly, Figs. 17 and 18 illustrate the Tauc plot for the allowed and forbidden transitions in PS/TiO₂ nanocomposites prepared using electrospinning.

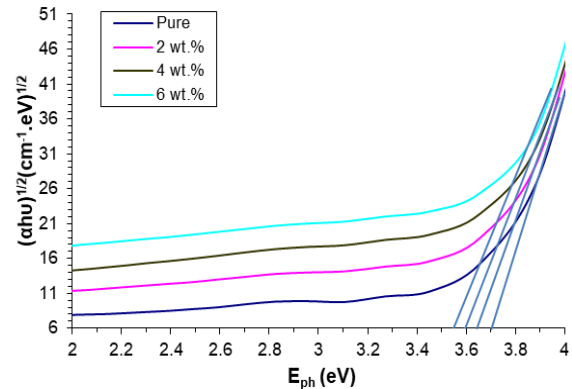


Fig. 17. The Tauc plot for pure PS and PS with different concentrations of TiO₂ NPs prepared by electrospinning. The extrapolation of the linear part is performed for the allowed transitions.

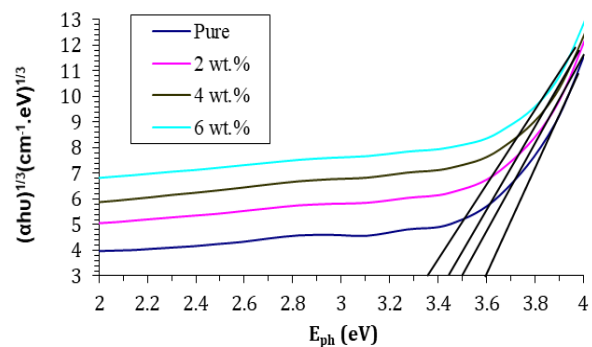


Fig. 18. The Tauc plot for pure PS and PS with different concentrations of TiO₂ NPs prepared by electrospinning. The extrapolation of the linear part is performed for the forbidden transitions.

Table 2. E_g^{opt} values for the allowed and forbidden indirect transition of pure PS and PS with different concentrations of TiO₂ NPs prepared by electrospinning.

Sample	Allowed (eV)	Forbidden (eV)
PS	3.7	3.6
PS/2 wt.% TiO ₂	3.6	3.5
PS/4 wt.% TiO ₂	3.55	3.4
PS/6 wt.% TiO ₂	3.52	3.38

Table 3. E_g^{opt} values for the allowed and forbidden indirect transition of pure PS and PS with different concentrations of TiO₂ NPs prepared by dip coating.

Sample	Allowed (eV)	Forbidden (eV)
PS	3.7	3.55
PS/2 wt.% TiO ₂	3.65	3.48
PS/4 wt.% TiO ₂	3.6	3.40
PS/6 wt.% TiO ₂	3.55	3.35

The data presented in Tables 2 and 3 illustrate a decrease in the band gaps of the studied nanocomposites for both allowed and forbidden indirect transitions with increasing the concentration of TiO₂ NPs. The observed behavior of the optical band gap can be attributed to the formation of energy levels within the energy gap.

The scheme of the electron transitions in the studied nanocomposite can be the following. The electron transition occurs in two distinct steps: firstly, from the valence band to the localized levels within the energy gap, and subsequently, from these localized levels to the conduction band. This transition is facilitated by increasing the concentration of TiO₂ nanoparticles.

It is worth noting that the electronic conductivity depends on the concentrations of these nanoparticles. The observed peculiarities correlate well with the results of previous investigations [35, 36]. The E_g^{opt} values for the allowed and forbidden indirect transition of pure PS and PS/TiO₂ nanocomposites prepared by dip coating and electrospinning show that the fabrication process had an inconsiderable impact on the energy of the band gap. In this case, the E_g^{opt} values for the allowed and forbidden indirect transition of PS fabricated using electrospinning are respectively 3.7 and 3.6 eV, which are approximately similar to the ones for the PS synthesized using dip coating. Other samples prepared using dip coating and electrospinning reveal the same behavior. The PS and PS/TiO₂ nanocomposites obtained using electrospinning reported in [26] exhibited optical band gaps of 4.54 and 4.45 eV, which are higher than the ones obtained in our study. Lower band gap energy is more favorable for optical applications since it simplifies the transition from the valence band to the conduction band.

4. Conclusions

This study effectively investigated the influence of TiO₂ NPs in PS. The studied PS/TiO₂ nanocomposites were fabricated using dip coating and electrospinning. The XRD analysis of PS/TiO₂ nanocomposites showed the amorphous structure of PS and the absence of peaks attributed to TiO₂ NPs. The FTIR analysis indicates the absence of any discernible chemical bonding between the TiO₂ NPs and the polymer matrix. The AFM analysis demonstrated that the polymer network exhibited a surface that was smooth and characterized by a uniform distribution of TiO₂ NPs. Furthermore, there was observed an increase in the surface roughness and average diameter with increasing the concentration of TiO₂ NPs.

It was ascertained that introducing the TiO₂ nanoparticles into PS has resulted in a decrease in the band gap energy compared to free TiO₂. Particularly, increasing the concentration of TiO₂ nanoparticles from 2 wt.% to 6 wt.% leads to a decrease in the band gap energy, which is caused by shortening in the distance from the valence band to the conduction band and simplifying the transition between these layers. The developed optical properties of the fabricated PS/TiO₂ composites in this work can be used in photocatalytic applications, namely the degradation of dyes in wastewater or photoelectrochemical uses like solar cells.

References

- Al-Seady M.A., Hossain M.M., Al-Mulali F.M., Shaik A.A. Prospective utilization of boron nitride and beryllium oxide nanotubes for Na, Li, and K-ion batteries: a DFT-based analysis. *J. Mol. Model.* 2023. **29**, Issue 11. P. 1–20. <https://doi.org/10.1007/s00894-023-05752-9>.
- Kadhim Q.S., Ahmad A., Ali F.A., Murtadha F.A. Effect of metal ad-atoms on the structural, electrical, and optical properties of boron-nitride nanostructures towards optoelectronics: a DFT based study. *Egypt. J. Chem.* 2022. **65**, Issue 13. P. 745–752. <https://doi.org/10.21608/ejchem.2022.130936.5763>.
- Al-Aaraji N.A.-H., Al-Seady M.A., Madlol H.A. *et al.* Investigation of pure and Al-doped graphene nanomaterials for toxic gas detection using first principles study. *IOP Conf. Ser. Earth Environ. Sci.* 2022. **1088**, Issue 1. P. 012013. <https://doi.org/10.1088/1755-1315/1088/1/012013>.
- Madlol H.A., Salman J.M., Abduljalil H.M. *et al.* Comparative adsorption calculations for CO and HCN gas interactions with graphene using density functional theory. *Egypt. J. Chem.* 2022. **65**, Issue 131. P. 385–391. <https://doi.org/10.21608/ejchem.2022.120895.5420>.
- Jasim S.A., Ahmed E., Al-Ghazaly S.M. *et al.* Adsorption ability of pure single-walled carbon nanotubes for toxic gas detection using DFT calculations. *AIP Conf. Proc.* 2022. **2398**, Issue 1. <https://doi.org/10.1063/5.0093549>.

6. Hashim A., Hadi A., Ibrahim H., Rashid F.L. Fabrication and enhancement of morphological and optical properties of PVP/SiC/Ti nanosystems for renewable energies and nanoelectronics. *J. Inorgan. Organometal. Polym. Mater.* 2023. P. 1–11. <https://doi.org/10.1007/s10904-023-02908-1>.
7. Abed H.H., Al-Aaraji N.A.-H., Salman J.M. *et al.* Theoretical study on dye-sensitized solar cells using graphene quantum dots and curcumin, phthalocyanine dyes. *IOP Conf. Ser. Earth Environ. Sci.* 2022. **1088**, Issue 1. P. 012012. <https://doi.org/10.1088/1755-1315/1088/1/012012>.
8. Hashim A., Hadi A., Al-Aaraji N.A.-H. Fabrication and augmented electrical and optical properties of PMMA/CoFe₂O₄/ZnCoFe₂O₄ hybrid nanocomposites for quantum optoelectronics. *Opt. Quant. Electron.* 2023. **55**, Issue 8. P. 716. <https://doi.org/10.1007/s11082-023-04994-4>.
9. Al-Seady M.A., Abdulwahhab N.A., Abbood H.I., Abduljalil H.M. DFT study of chemical adsorption of NO₂ gas on graphene nanomaterials. *Mater. Sci. Forum.* 2021. **1039**. P. 391–397. <https://doi.org/10.4028/www.scientific.net/MSF.1039.391>.
10. Kik K., Bukowska B., Sicińska P. Polystyrene nanoparticles: sources, environmental occurrence, tissue distribution, accumulation, and toxicity. *Environ. Pollut.* 2020. **262**. P. 114297. <https://doi.org/10.1016/j.envpol.2020.114297>.
11. Al-Seady M.A., Ahmed E., Abduljalil H.M., Ekhewish A.A. Studying the adsorption energy of CO gas molecule in different nanosystems using density functional theory. *Egypt. J. Chem.* 2021. **64**, Issue 5. P. 2607–2612. <https://doi.org/10.21608/ejchem.2021.55434.3169>.
12. Ziental D., Czarczynska-Goslinska B., Mlynarczyk D.T. *et al.* Titanium dioxide nanoparticles: prospects and applications in medicine. *Nanomaterials.* 2020. **10**, Issue 2. P. 387. <https://doi.org/10.3390/nano10020387>.
13. Nyamukamba P., Okoh O., Mungondori H. *et al.* Synthetic methods for titanium dioxide nanoparticles: a review. *Titanium Dioxide – Material for a Sustainable Environment.* 2018. **8**. P. 151–175. <http://doi.org/10.5772/intechopen.75425>.
14. Rajput N. Methods of preparation of nanoparticles: a review. *Int. J. Adv. Eng. Technol.* 2015. **7**, Issue 6. P. 1806. <https://doi.org/10.4236/ojinm.2018.82002>.
15. Jamkhande P.G., Ghule N.W., Bamer A.H., Kalaskar M.G. Metal nanoparticles synthesis: overview of preparation methods, advantages and disadvantages, and applications. *J. Drug Deliv. Technol.* 2019. **53**. P. 101174. <https://doi.org/10.1016/j.jddst.2019.101174>.
16. Christian P., Von der Kammer F., Baalousha M., Hofmann T. Nanoparticles: structure, properties, preparation, and behavior in environmental media. *Ecotoxicology.* 2008. **17**. P. 326–343. <https://doi.org/10.1007/s10646-008-0213-1>.
17. Rao B.G., Mukherjee D., Reddy B.M. Novel approaches for nanoparticle preparation. In: *Nanostructures for Novel Therapy.* Elsevier, 2017. P. 1–36. <https://doi.org/10.1016/B978-0-323-46142-9.00001-3>.
18. Rao J.P., Geckeler K.E. Polymer nanoparticles: preparation techniques and size-control parameters. *Prog. Polym. Sci.* 2011. **36**, Issue 7. P. 887–913. <https://doi.org/10.1016/j.progpolymsci.2011.01.001>.
19. Sungur Ş. Titanium dioxide nanoparticles. In: *Hand-book of Nanomaterials and Nanocomposites for Energy and Environmental Applications.* 2021. P. 713–730. https://doi.org/10.1007/978-3-030-36268-3_9.
20. Mo S.-D., Ching W. Electronic and optical properties of rutile, anatase, and brookite phases of titanium dioxide. *Phys. Rev. B.* 1995. **51**, Issue 19. P. 13023. <https://doi.org/10.1103/PhysRevB.51.13023>.
21. Gowthaman N., Lim H., Sreeraj T., Amalraj A., Gopi S. Advantages of biopolymers over synthetic polymers: social, economic, and environmental aspects. In: *Biopolymers and Their Industrial Applications.* Elsevier, 2021. P. 351–372. <http://doi.org/10.1016/B978-0-12-819240-5.00015-8>.
22. Zhou D., Chen J., Wu J. *et al.* Biodegradation and catalytic-chemical degradation strategies to mitigate microplastic pollution. *Sustain. Mater. Technol.* 2021. **28**. P. e00251. <https://doi.org/10.1016/j.susmat.2021.e00251>.
23. Erdem B., Sudol E.D., Dimonie V.L., El-Aasser M.S. Encapsulation of inorganic particles via miniemulsion polymerization. II. Preparation and characterization of styrene miniemulsion droplets containing TiO₂ particles. *J. Polym. Sci. Part A: Polym. Chem.* 2000. **38**, Issue 24. P. 4431–4440. [https://doi.org/10.1002/1099-0518\(20001215\)38:24%3C4431::AID-POLA120%3E3.0.CO;2-Y](https://doi.org/10.1002/1099-0518(20001215)38:24%3C4431::AID-POLA120%3E3.0.CO;2-Y).
24. Toyama N., Takahashi T., Terui N., Furukawa S. Synthesis of polystyrene@TiO₂ core-shell particles and their photocatalytic activity for methylene blue decomposition. *Inorganics.* 2023. **11**, Issue 8. P. 343. <https://doi.org/10.3390/inorganics11080343>.
25. Hayri-Senel T., Kahraman E., Sezer S. *et al.* Photocatalytic degradation of ciprofloxacin from water using waste polystyrene and TiO₂ composites. *Heliyon.* 2024. **10**, Issue 3. P. e25433. <https://doi.org/10.1016/j.heliyon.2024.e25433>.
26. Jaleh B., Madad M.S., Tabrizi M.F. *et al.* UV-degradation effect on optical and surface properties of polystyrene-TiO₂ nanocomposite film. *J. Iran. Chem. Soc.* 2011. **8**. P. S161–S168. <https://doi.org/10.1007/BF03254293>.
27. Schinke C., Rattana S., Ziletti A., Oganov A.R. Uncertainty analysis for the coefficient of band-to-band absorption of crystalline silicon. *AIP Adv.* 2015. **5**, Issue 6. <https://doi.org/10.1063/1.4923379>.
28. Makuła P., Pacia M., Macyk W. How to correctly

- determine the band gap energy of modified semiconductor photocatalysts based on UV-Vis spectra. *ACS Publ.* 2018. **9**. P. 6814–6817. <https://doi.org/10.1021/acs.jpcelett.8b02892>.
29. Jachak M., Bhise R., Chaturvedi A. *et al.* Pyrroloquinoline based styryl dyes doped PMMA, PS, and PS/TiO₂ polymer for fluorescent applications. *J. Inorgan. Organometal. Polym. Mater.* 2022. **32**, Issue 7. P. 2441–2454. <https://doi.org/10.1007/s10904-022-02285-1>.
 30. Costa R.G., Bricchi G.S., Ribeiro C., Mattoso L.H. Nanocomposite fibers of poly(lactic acid)/titanium dioxide prepared by solution blow spinning. *Polymer Bulletin.* 2016. **73**, Issue 11. P. 2973–2985. <https://doi.org/10.1007/s00289-016-1635-1>.
 31. Sen P., Suresh K., Kumar R.V. *et al.* A simple solvent blending coupled sonication technique for synthesis of polystyrene (PS)/multi-walled carbon nanotube (MWCNT) nanocomposites: effect of modified MWCNT content. *J. Sci.: Adv. Mater. Devices.* 2016. **1**, Issue 3. P. 311–323. <https://doi.org/10.1016/j.jsamd.2016.06.016>.
 32. Litina K., Kallitsis J.K., Zamboulis D., Vasilakaki M. Nanocomposites of polystyrene-b-polyisoprene copolymer with layered silicates and carbon nanotubes. *Eur. Polym. J.* 2006. **42**, Issue 9. P. 2098–2107. <https://doi.org/10.3390/polym13050745>.
 33. Chiu F.-C., Li B.-H., Jiang J.-Y. Syndiotactic polystyrene/multi-walled carbon nanotube nanocomposites: polymorphism, thermal properties, electrical conductivity, and rheological properties. *Compos. – A: Appl. Sci. Manuf.* 2012. **43**, No 12. P. 2230–2240. <https://doi.org/10.1016/j.compositesa.2012.08.002>.
 34. Al-Seady M.A., Grmasha R.A., Al-Aaraji N.A.-H., Abduljalil H.M. Investigation of the adsorption mechanism of methane gas in graphene and copper-doped nano-ribbon using density function theory. *J. Phys.: Conf. Ser.* 2021. **1879**, Issue 3. P. 032099. <http://doi.org/10.1088/1742-6596/1879/3/032099>.
 35. Gaabour L. Effect of the addition of TiO₂ nanoparticles on structural and dielectric properties of polystyrene/polyvinyl chloride polymer blend. *AIP Adv.* 2021. **11**, Issue 10. <https://doi.org/10.1063/5.0062445>.
 36. Meftah Y., Bekker D., Benhaoua B. *et al.* Post-annealing effect on structural and optical properties of (α -Fe₂O₃) thin films prepared by spray pyrolysis with moving nozzle. *Digest J. Nanomater. Biostruct.* 2018. **13**. P. 465–474.
 37. Hassanien A.S., Akl A.A. Optical characteristics of iron oxide thin films prepared by spray pyrolysis technique at different substrate temperatures. *Appl. Phys. A.* 2018. **124**, Issue 11. P. 752. <https://doi.org/10.1007/s00339-018-2180-6>.
 38. Habeeb M.A., Hashim A., Mohammed R.M. Preparation and investigation of structural and dielectric properties of PEO-PVA-Fe₂O₃ nanocomposites for electronic nanodevices. *Nanosystems, Nanomaterials, Nanotechnologies.* 2023. **21**, Issue 3. <https://doi.org/10.15407/nmn.21.03.513>.
 39. Kadhim A.F., Hashim A. Fabrication and augmented structural optical properties of PS/SiO₂/SrTiO₃ hybrid nanostructures for optical and photonics applications. *Opt. Quant. Electron.* 2023. **55**, No 5. P. 432. <https://doi.org/10.1007/s11082-023-04699-8>.

Authors and CV



Sfeer Abdulkareem Abdulreem Al-Saati, Assistant Professor, researcher at the Faculty of Basic Education, Department of Science, University of Babylon, Iraq. He defended his Master's thesis in Physics, Mansoura University, Egypt Faculty of Science, 2015, specialization: experimental physics. With over 15 publications, his scientific interests span a wide range of fields, particularly physics, nanomaterials and the environment and pollution. PhD student, University of Sfax, Faculty of Sciences.
E-mail: safeer263601@gmail.com,
<http://orcid.org/0000-0002-0691-7894>



Najmeddine Abdelmoula is Full Professor, Senior Researcher at the Faculty of Sciences of Sfax, University of Sfax, Tunisia. He defended his Ph.D. thesis in physics, specializing in materials science, in 2001 at the Faculty of Sciences of Sfax, and obtained his habilitation in physics in 2007 at the University of Sfax. With over 135 publications, his scientific interests span a wide range of fields, particularly physics and technological devices based on magnetic, dielectric, piezoelectric, and multifunctional materials.
E-mail: Najmeddine.abdelmoula@fss.rnu.tn,
<https://orcid.org/0000-0002-6318-9547>



Mohammed Hadi Shinen AL-Darwish is Professor, Senior Researcher at the Faculty of Sciences of Babylon, University of Babylon, Iraq. He defended his Ph.D. thesis in physics, specializing in materials science, in 2011 at the Faculty of Sciences of Basrah and Sheffield Hallam.

With over 77 publications and 23 of Conference, his scientific interests span a wide range of fields, particularly physics and physics materials (nano thin film)/solar cell and sensor.
E-mail: mohammed.shinen@yahoo.com

Authors' contributions

AL Saati S.A.A.: formal analysis, investigation, data curation (partially), writing – original draft, visualization, writing – review & editing.

Abdelmoula N.: conceptualization, methodology, validation, formal analysis, investigation, resources, data curation, writing – original draft, writing – review & editing.

Shinen M.H.: conceptualization, investigation, project administration, writing – review & editing.

Порівняння структурних, морфологічних та оптичних властивостей нанокompозитних плівок PS/TiO₂, виготовлених методами занурення та електропрядіння

S.A.A. AL Saati, N. Abdelmoula and M.H. Shinen

Анотація. Це дослідження містить процедуру синтезу чистого полістиролу (ПС) і нанокompозитів ПС/TiO₂ з різними концентраціями (2, 4 і 6 мас.%) наночастинок діоксиду титану (НЧ TiO). НЧ TiO були виготовлені за допомогою методів занурення та електропрядіння. Рентгенівський дифракційний аналіз (XRD) показав, що полістирол є аморфним, і чітких піків, що відповідають наночастинкам TiO, не виявлено. Аналіз інфрачервоної Фур'є спектроскопії (FTIR) показав, що помітна взаємодія між наночастинками TiO та ПС відсутня. Аналіз за допомогою атомно-силової мікроскопії (АСМ) продемонстрував, що вбудовані у ПС наночастинки TiO мають нерівномірний розподіл по поверхні. Як свідчать зображення, отримані скануючою електронною мікроскопією (SEM), у приготованих методом занурення зразках спостерігаються агломеровані та шаруваті сферичні частинки. Але зразки, синтезовані методом електропрядіння, показали, що НЧ TiO були добре розділені, і в цих зразках не було виявлено жодних агломерацій, пов'язаних з НЧ TiO. Відповідно до результатів видимої та ультрафіолетової спектроскопометрії, обидва зразки, підготовлені методами занурення та електропрядіння, показали позитивну кореляцію між концентрацією наночастинок TiO та поглинанням. Збільшення об'ємної частки наночастинок TiO привело до зменшення ширини забороненої зони зразків, виготовлених методами занурення та електропрядіння, що означає, що електронний перехід від валентної зони до зони провідності спрощується завдяки збільшенню концентрації наночастинок TiO₂.

Ключові слова: нанокompозит ПС/TiO₂, метод занурення, метод електропрядіння, оптичні властивості, полістирол, TiO₂.